Photoproduction of multi-meson final states – recent results from the Crystal-Barrel/TAPS experiment at ELSA-*

U. Thoma[1)] (for the CBELSA/TAPS collaboration)

(HISKP, Universität Bonn, Nussallee 14-16, 53115 Bonn, Germany)

Abstract Multi-meson final states such as $\gamma p \to p\pi^0\pi^0$ and $\gamma p \to p\pi^0\eta$ have been investigated with the Crystal-Barrel/TAPS experiment at ELSA. Baryon cascades via $\Delta\pi$ and $\Delta\eta$ and also via higher mass baryon resonances are clearly observed. Based on this data and on data from other reactions a partial wave analysis has been performed from which partial decay widths of various N^* and Δ^* states into the different $p\pi^0\pi^0$ and $p\pi^0\eta$ decay channels have been determined, leading partly to unexpected results. In addition, polarisation observables have been investigated. The beam asymmetry Σ has been determined for both reactions and double polarisation data using a longitudinally polarised target and a circularly or linearly polarised photon beam has been taken. Given the angular coverage of the Crystal-Barrel/TAPS experiment this data covers almost the full angular range and phase space. This data will provide new and important information for the partial wave analyses and bring us one step closer towards a complete experiment.

Key words baryon spectroscopy, photoproduction, multi-meson final states, polarisation observables

PACS 13.30.-a, 13.40.-f, 13.60.Le

1 Introduction

To understand the non-perturbative regime of QCD – the world of the nucleon and its excitations – is still among the most exciting challenges in subnuclear physics. In the past most of the information on the baryon excitation spectrum was obtained from πN-scattering experiments putting a clear bias on resonances with a sizeable πN-coupling. Recently this data was supplemented by photo- and electroproduction data, which offers the opportunity to study resonances with vanishing πN-coupling in reactions such as e.g. $\gamma p \to p\eta$. To extract the broad and strongly overlapping resonances from the data two issues are rather important: First of all, polarisation observables need to be measured to gain enough constraints for an unambiguous extraction of the contributing amplitudes from the data. Secondly, different final states need to be investigated since different resonances may couple with rather different strength to different final states making their observation more probable in certain reactions compared to others. This of course includes measurements of single-meson photoproduction reactions as well as the more complicated multi-meson photoproduction. The latter gets more and more important at higher energies. This is visible in Fig. 1 which shows the total cross sections for various final states in comparison to the total photoabsorption cross section.

Multi-meson final states allow the investigation of resonances decaying e.g. via $\Delta(1232)\pi$ or $\Delta(1232)\eta$. The measurement of such decay modes or decay modes in general provides important information to distinguish between different models trying to describe the baryon spectrum such as e.g. the quark model or calculations investigating the option of dynamically generated resonances. These results do also provide a testing ground for future lattice QCD calculations. The ground state baryons and the low–mass excitations evidence the decisive role of $SU(3)$ symmetry and suggest an interpretation of the spectrum in constituent quark models[1—3]. Baryon decays can

Received 7 August 2009

* Supported by German Science Foundation (DFG) in the frame of the SFB/TR16

1) E-mail: thoma@hiskp.uni-bonn.de

be calculated in quark models using harmonic–oscillator wave functions and assuming a $q\bar{q}$ pair creation operator for meson production. A comprehensive review of predictions of baryon masses and decays can be found in Ref. [4]. An alternative description of the baryon spectrum may be developed in effective field theories in which baryon resonances are generated dynamically from their decays[5, 6]. At present, the approach is restricted to resonances coupling to octet baryons and pseudoscalar mesons, yet it can possibly be extended to include vector mesons and decuplet baryons[7]. To test the different approaches, detailed information on the spectrum and decays of resonances is needed, including more complex decay modes such as e.g. $\Delta\pi$, $\Delta\eta$ or N($\pi\pi$)-S-wave.

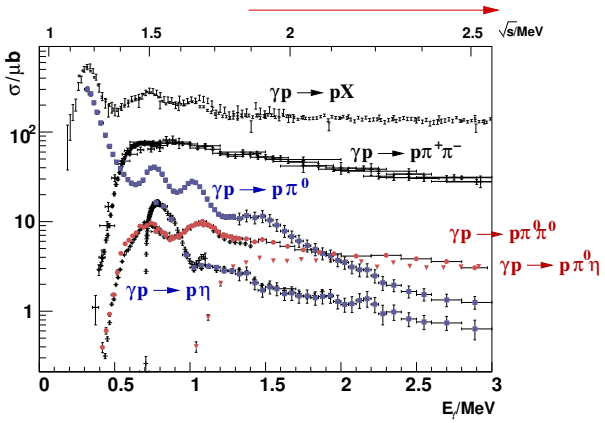

Fig. 1. Total photoabsorption cross section in comparison to various single- and double-meson photoproduction cross sections.

2 The multi-meson final states $\gamma p \to p\pi^0\pi^0, \gamma p \to p\pi^0\eta$

Multi-meson final states like $\gamma p \to p\pi^0\pi^0$ and $\gamma p \to p\pi^0\eta$ provide important tools to study the decay dynamics of highly excited baryon resonances. Data were taken by the CB-ELSA experiment in two run periods, with an electron beam energy of 1.4 and 3.2 GeV, respectively. The low-energy run covered the second and third resonance region and invariant masses up to about 1.8 GeV. The high-energy run covers baryon resonances with masses up to 2.5 GeV. Fig. 2 shows for p4γ-events the $\gamma\gamma$-invariant mass of one two-photon-pair plotted versus the $\gamma\gamma$-invariant mass of the other two-photon-pair[8]. Peaks due to the reactions $\gamma p \to p\pi^0\pi^0$ and $\gamma p \to p\pi^0\eta$ are clearly observed. The π^0 is reconstructed with a resolution σ_{π^0}=8 MeV. Extensive Monte-Carlo simulations have shown that the background to the $p\pi^0\pi^0$-final state is below 1% (2%) for the low (high) energy data set.

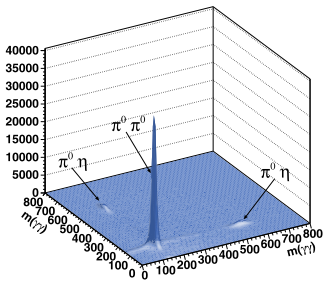

Fig. 2. $\gamma\gamma$-invariant mass distribution of one photon pair versus the invariant mass distribution of the second photon pair after a kinematic fit to $\gamma p \to p4\gamma$ (6 entries per event) for data from the high-energy run.

1) $\gamma p \to p\pi^0\pi^0$

Figure 3 shows the CB-ELSA results on the unpolarised $p\pi^0\pi^0$-photoproduction up to $\sqrt{s} \leqslant 1.8$ GeV[8] together with the result of the fit within the BnGa-partial wave analysis (for further details on the BnGa-PWA see Ref. [9]).

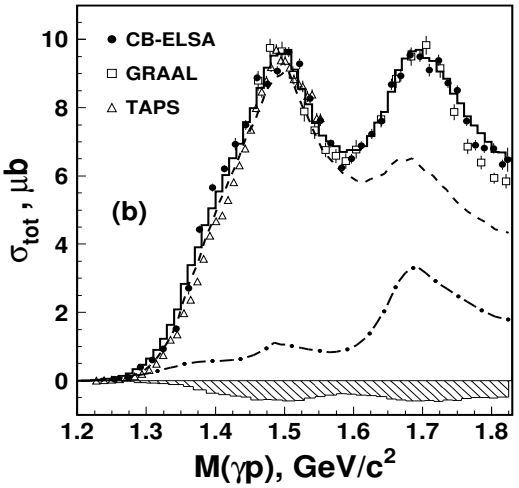

Fig. 3. Total cross section for $\gamma p \to p\pi^0\pi^0$ (low energy data set). Solid line: Result of the fit (BnGa-PWA), band below the figure: systematic error. Dashed curve: $\Delta^+\pi^0 \to p\pi^0\pi^0$, dashed-dotted line: $p(\pi^0\pi^0)_S$ cross section as derived from the PWA. The D_{33} partial wave gives the strongest contribution to the second resonance region, followed by D_{13}. The D_{13} – D_{33} interference generates the dip between the second and third resonance region.

The data has been subject to the BnGa-PWA which included in addition to the discussed data set also various data sets on single-meson photoproduction as well as specific waves from elastic πN scattering. In addition, data from Crystal Ball on

$\pi^- p \to n2\pi^0$ was included in the fit[11]. All three-particle final states were fitted in terms of an event-based maximum likelihood fit, which is the only way to properly take into account all the information included in the correlations between the five variables the reaction depends on. From the fits the properties of the contributing N* and Δ^* resonances have been extracted and their partial decay widths into the different $p\pi^0\pi^0$ decay modes, such as $\Delta(1232)\pi$, $N(\pi\pi)_S$–wave, $P_{11}(1440)\pi$, and $D_{13}(1520)\pi$ have been determined (for further details see Refs. [8, 10]). Several of these partial widths were determined for the first time.

An interesting pattern of partial decays of resonances into $\Delta\pi$, not expected by quark model calculations nor by naive phase space arguments, is observed. D_{13}-decays into $\Delta\pi_{S-\mathrm{wave}}$ are allowed by all selection rules but are observed to be weaker than naively expected. The $D_{13}(1520)$ decays into $\Delta\pi$ in D-wave are observed with about the same strength as in S-wave even though D-wave decays should be suppressed at such small momenta (~ 250 MeV/c). The $D_{13}(1700)$ $\Delta\pi_{S-\mathrm{wave}}$ decay is observed to be weaker than $\Delta\pi_{D-\mathrm{wave}}$.

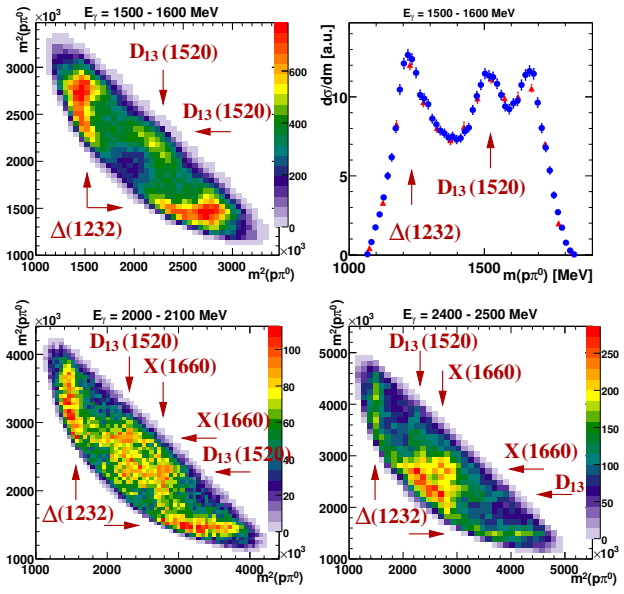

Fig. 4. $\gamma p \to p\pi^0\pi^0$: Dalitz plots and differential cross section distribution in arbitrary units for different tagged photon energy ranges as indicated above the figures.

For the $D_{33}(1700)$ two distinct ambiguous solutions have been found; for one of them the S-wave, for another one the D-wave, dominates. So it remains presently unclear whether only the N*-states, $D_{13}(1520)$ and $D_{13}(1700)$, or also the Δ^*-states with $J^P = 3/2^-$ show this unexpected decay pattern. Double polarisation experiments as presently performed at the electron stretcher ring ELSA[20] in Bonn are urgently needed. They will help to resolve this ambiguity. The sensitivity which can be expected from one of the according measurements of polarisation observables is discussed in section 2.3.2.

In a preliminary PWA which includes also the high energy CB-ELSA data set (up to E_γ=3.0 GeV) a clear evidence for baryon cascades has been found. Resonances in the intermediate state are already clearly visible by eye in Fig. 4, which shows the higher statistic CBELSA/TAPS data. In the intermediate state the $\Delta(1232)$, the $D_{13}(1520)$ and an additional state around 1660 MeV are observed. In addition, the $f_2(1270)$ and the $f_0(980)$ contribute. The strong occurrence of high mass resonances in the data and in the decay of baryon resonances (PWA) may indicate that QCD prefers to invest in mass rather than in momentum.

2) $\boldsymbol{\gamma p \to p\pi^0\eta}$

The reaction $\gamma p \to p\pi^0\eta$ includes the isospin selective $\Delta\eta$ intermediate state from which information on excited Δ^*-states can be obtained. In the $\Delta\eta_{S-\mathrm{wave}}$, the $\Delta^*(1700)$ and $\Delta^*(1940)$ could play a similar role as the S_{11} resonances in the $N\eta_{S-\mathrm{wave}}$. So far, $\Delta^*(1940)$ is only a one-star resonance in the PDG classification[12]).

The reaction was analysed using the high-energy data from the CB-ELSA run period (for further details see Refs. [13, 14]). The BnGa-PWA (see also Fig. 5) finds strong contributions from the P_{33} and D_{33} partial waves. The latter partial wave is particularly exciting: it contains two, possibly three, resonances, $\Delta(1700)$, $\Delta(1940)$, and possibly a weak $\Delta(2350)$ contribution. The $\Delta(1940)$ is particular interesting. It confirms the one-star $\Delta(1940)$ which may belong to a triplet of states lying significantly below the expectation of symmetric quark models.

The $D_{33}(1940)$ and the $P_{33}(1920)$ both contributing to the $\gamma p \to p\pi^0\eta$-channel have opposite parity and very similar masses. A parity doublet occurs. This might indicate that resonances in the Δ^* spectrum with alternating parities may have similar masses rather than following a $2n+l$ behaviour. More information on the baryon spectrum is urgently needed. As in the $p\pi^0\pi^0$ final state baryon cascades are also observed in the reaction $\gamma p \to p\pi^0\eta$. Here, as visible in Fig. 6, the $\Delta(1232)$, the $S_{11}(1535)$ and the $a_0(980)$ are clearly observed in the according Dalitz plots and invariant masses.

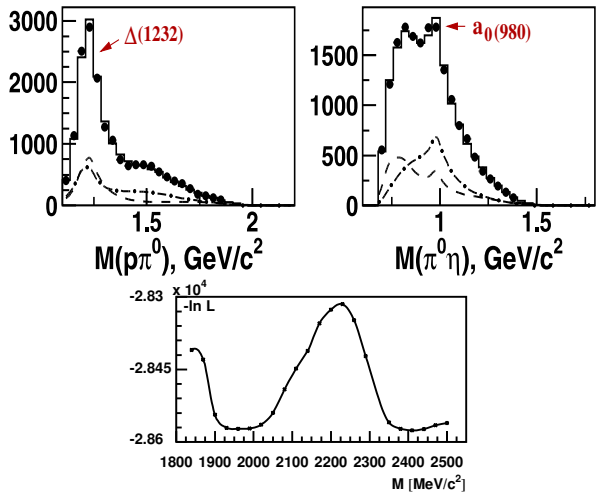

Fig. 5. Quality of the data description by the PWA, showing two invariant mass distributions as example. Data are represented by dots, the fit as solid line. Errors are statistical nature only. The dashed line stands for the D_{33}-, the dashed-dotted line for the P_{33}-partial wave. The distributions are not corrected for acceptance to allow a fair comparison of the fit with the data without introducing any model dependence by extrapolating e.g. over acceptance holes. Clearly visible are the $\Delta(1232)$ and the $a_0(980)$. The lower picture shows the minimum in the likelihood scan if the mass of a second D_{33} introduced in addition to the $D_{33}(1700)$ is varied.

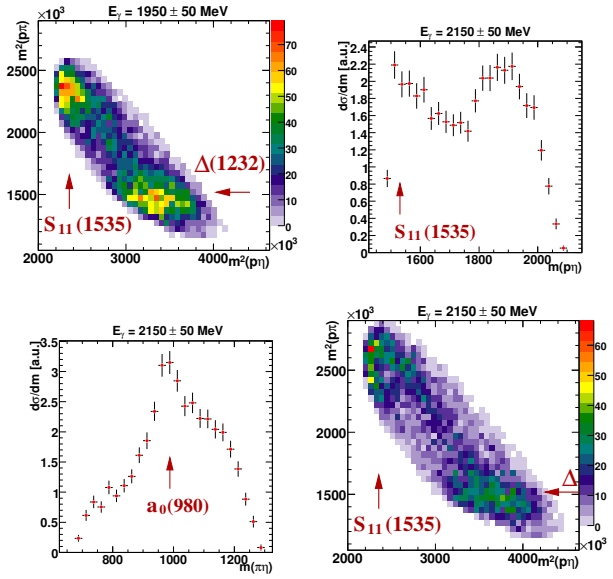

Fig. 6. $\gamma p \rightarrow p\pi^0\eta$: Dalitz plots for different tagger photon energy ranges as indicated above the figure and differential cross sections given in arbitrary units.

In the PWA, decays of baryon resonances via these intermediate resonances are observed to contribute to the reaction $\gamma p \rightarrow p\pi^0\eta$.

2.1 Polarisation observables

In contrast to single pseudoscalar meson photoproduction, where 8 carefully chosen observables need to be measured to reach a complete experiment (see Ref. [15] and also Ref. [16]), 15 observables[18] have to be determined in case of the photoproduction of two pseudoscalar mesons. This is due to fact that the reaction is no longer restricted to a single plane as visible in Fig. 7, but two planes, a reaction and a decay plane, are of importance.

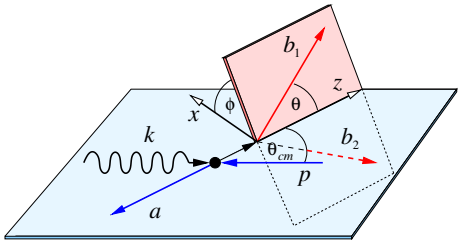

Fig. 7. Photoproduction of a three particle final state, shown are the reaction plane including the incoming photon and proton and a final state particle and the decay plane including the final state particles b_1 and b_2. Figure taken from Ref. [19].

This leads to the fact that polarisation asymmetries can also occur if e.g. only the beam is circularly polarised or if only the target is longitudinally polarised. Being restricted to only the reaction plane, those asymmetries do not occur in single pseudoscalar meson photoproduction.

2.2 Measurement of the beam asymmetry Σ

One of the polarisation observables of interest is the single polarisation observable Σ which will be discussed in the following. In case of a linearly polarised photon beam and an unpolarised target, the cross section for the photoproduction of two pseudoscalar mesons can be written in the form

$$\frac{\mathrm{d}\sigma}{\mathrm{d}\Omega} = \left(\frac{\mathrm{d}\sigma}{\mathrm{d}\Omega}\right)_0 \left(1 + \delta_l \left(\Sigma \cos 2\Phi + I^{\mathrm{S}} \sin 2\Phi\right)\right), \quad (1)$$

where $\left(\frac{\mathrm{d}\sigma}{\mathrm{d}\Omega}\right)_0$ denotes the cross section in case of an unpolarised photon beam, δ_l the degree of linear polarisation of the photon beam, Σ and I^{S} the occurring polarisation observables, and Φ the angle between the polarisation plane and the normal to the reaction plane.

In the CBELSA/TAPS experiment the linearly polarised photons are produced via coherent

bremsstrahlung of the initial 3.2 GeV electron beam delivered by ELSA off a diamond radiator. Electrons undergoing the bremsstrahl process are then momentum analysed using a tagging spectrometer consisting of a dipole magnet and a scintillator based detection system. For further details on the experimental setup, see Ref. [21].

For the given analysis, two datasets were considered. Fig. 8 shows the degree of polarisation as a function the incident photon energy for two diamond radiator orientations, one yielding a maximum degree of polarisation of 49.2% at $E_\gamma = 1300$ MeV (A) and the other of 38.7% at 1600 MeV (B).

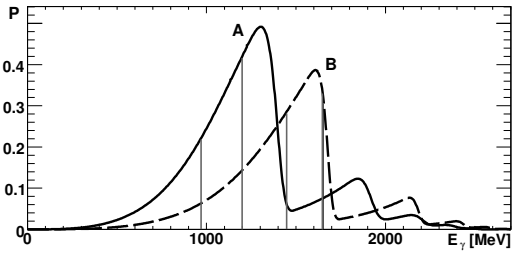

Fig. 8. Degree of linear polarisation for the two different settings. Maximum degrees of polarisation were 49.2% at $E_\gamma = 1300$ MeV (A) and 38.7% at 1600 MeV (B) respectively. Vertical lines indicate the energy ranges under consideration.

To extract the polarisation observables according to Eq. (1) a fit on the Φ distribution of the final state particles was performed.

1) $\vec{\gamma}\mathrm{p} \to \mathrm{p}\pi^0\pi^0$

Figure 9 shows preliminary results for the beam asymmetries Σ extracted for the $\vec{\gamma}\mathrm{p} \to \mathrm{p}\pi^0\pi^0$-channel (for further details see Ref. [22]). Clearly visible is an energy and an angular dependence. The beam asymmetry tends to be largest in the lowest energy bin measured. The agreement with the previously published data points from GRAAL[23] is reasonable even though especially in the $\Sigma(p)(m(\pi^0\pi^0))$-distributions deviations are observed. These might be due to the different areas of the five-dimensional phase space covered by the two experiments. This is presently subject to further investigations.

2) $\vec{\gamma}\mathrm{p} \to \mathrm{p}\pi^0\eta$

Figure 10 shows examples for the beam asymmetries Σ extracted for the $\vec{\gamma}\mathrm{p} \to \mathrm{p}\pi^0\eta$-channel (for further details see Refs. [24, 25]). Asymmetries up to an order of 40%—50% can be clearly observed as well as a distinct difference in the sign of the asymmetry derived from the Φ distribution of the η meson and the proton, respectively. An energy dependence, especially for the asymmetries as function of the $\mathrm{p}\pi^0$ invariant mass is also visible. The data are compared with a prediction of the Bonn-Gatchina partial wave analysis (PWA)[27, 28]. The solution shown has been determined from a PWA of the unpolarised CB-ELSA $\gamma\mathrm{p} \to \mathrm{p}\pi^0\eta$ data fitted in combination with additional datasets[13, 14]. The data presented here were not incorporated. A general agreement between the data and the prediction is noticeable, tendencies and signs are widely reproduced, even though there is obviously room for improvement. First fits including this data are consistent with the need for the $D_{33}(1940)$ observed in the fit to the unpolarised data. A comparison with the GRAAL data[26] for this reaction, covering an incoming photon energy range of 1.1—1.5 GeV, shows a more than reasonable agreement within the errors and given the different energy binning.

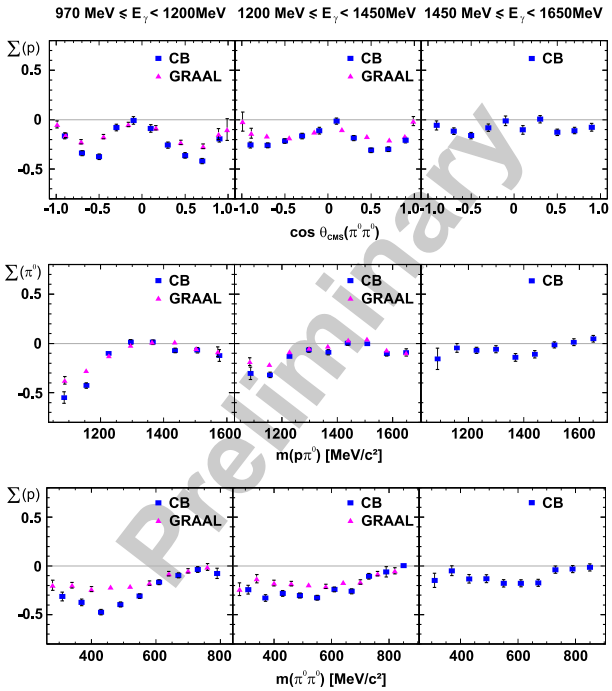

Fig. 9. Measured beam asymmetries Σ in the reaction $\vec{\gamma}\mathrm{p} \to \mathrm{p}\pi^0\pi^0$. Left to right: Incoming photon energy ranges 1085 ± 115 MeV, 1325 ± 125 MeV, 1550 ± 100 MeV for the CBELSA/TAPS data. First row: Beam asymmetries obtained from the Φ-distribution of the proton as a function of $\cos\Theta_{\mathrm{cms}}$ of the $\pi^0\pi^0$ system. Second row: Obtained from the Φ-distribution the π^0 as a function of the $\mathrm{p}\pi^0$ invariant mass. Third row: Obtained from the Φ-distribution of the proton as a function of the $\pi^0\pi^0$ invariant mass. The GRAAL data cover incoming photon energies up to 1450 MeV.

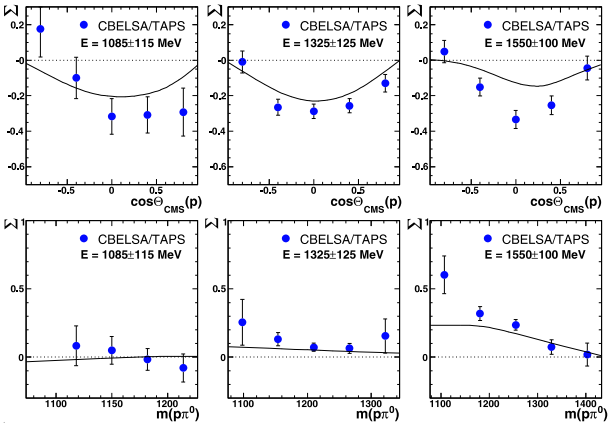

Fig. 10. Measured beam asymmetries Σ in the reaction $\vec{\gamma}p \to p\pi^0\eta$. Left to right: Incoming photon energy ranges 1085 ± 115 MeV, 1325 ± 125 MeV, 1550 ± 100 MeV. Upper row: Beam asymmetries obtained from the Φ distribution of the proton as a function of $\cos\Theta_{\rm CMS}$ of the proton, lower row: beam asymmetries obtained from the Φ distribution of the η as a function of the $p\pi^0$ invariant mass. Solid line: Bonn-Gatchina PWA prediction. The GRAAL data are not shown because of a different energy binning.

2.3 Double polarisation measurements

Significant progress in understanding the baryon excitation spectrum can clearly not be expected without extensive information on polarisation observables. One important step forward is without doubt the measurement of double polarisation observables. First measurements using a longitudinally polarised target and a linearly or circularly polarised photon beam have recently started at ELSA (for single-pseudoscalar-meson photoproduction see Ref. [16], for ω-photoproduction see Ref. [17]) using the setup discussed in the following.

2.3.1 Experimental setup

The double polarisation measurements have been performed using the Bonn-frozen-spin butanol target[29]. During the measurements a typical mean polarisation of 70% and relaxation times around 600 h have been reached. Circularly polarised photons have been obtained by bremsstrahlung of longitudinally polarised electrons on an amorphous radiator. At 2.4 GeV electron energy an electron beam polarisation ∼65% has been measured at the Moeller target. Linearly polarised photons are again been obtained using the method of coherent bremsstrahlung off a diamond radiator.

The experimental setup used to perform the experiments is shown in Fig. 11. The Crystal Barrel calorimeter consists of 1230 CsI(Tl)-crystals and is complemented by two further calorimeters; the forward detector and the MiniTAPS array. The forward detector consists of 90 CsI(Tl) crystals covering the angular range between 30° and 12°. The MiniTAPS array (216 BaF_2-crystals) covers the angular range further down to 1.2°. While the Crystal Barrel CsI(Tl)-crystals are read out by photodiodes, for the forward detector crystals photomultipliers are utilised. These give the forward detector trigger capabilities and allow timing measurements. The time resolution achieved with this crystal-lightguide-photomultiplier configuration is about 4 ns (FWHM) which is sufficient for its inclusion in the first level trigger. Plastic scintillators are placed in front of the crystals of both forward detectors to identify charged particles. For the forward detector a double layer of 180 plastic scintillators of 3 mm thickness is placed in front of the crystals. The front faces of MiniTAPS BaF_2 crystals are also covered by plastic scintillator plates. For charged particle detection a fibre detector consisting of three layers of in total 513 fibres (orientation: $\pm 25°, 0°$) is installed inside the Crystal Barrel calorimeter. This arrangement allows the reconstruction of the penetration point of the charged trajectory with the inner detector. To suppress electromagnetic background on the trigger level a CO_2-Gas-Čerenkov detector has been installed between the forward detector and MiniTAPS.

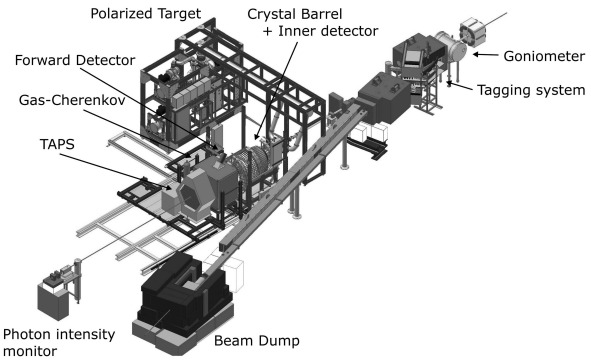

Fig. 11. The CBELSA/TAPS experimental setup together with the polarised target used for the recent double polarisation experiments.

This setup covers ∼96% of the 4π solid angle.

2.3.2 Sensitivity

Figure 12 shows an example of the strength of double polarisation experiments. As discussed before the solution of the BnGa-partial wave analysis shows an ambiguity[8]; the $D_{33}(1700)$ might either decay dominantly via ℓ=0 or ℓ=2. For those two solutions the helicity differences $\sigma_{1/2} - \sigma_{3/2}$ have been

calculated. Large differences in the total as well as in the differential cross sections are observed showing the sensitivity such a measurement would have. First double polarisation data has been taken at ELSA and is presently analysed. Additional statistics will be gained in a forthcoming measurement.

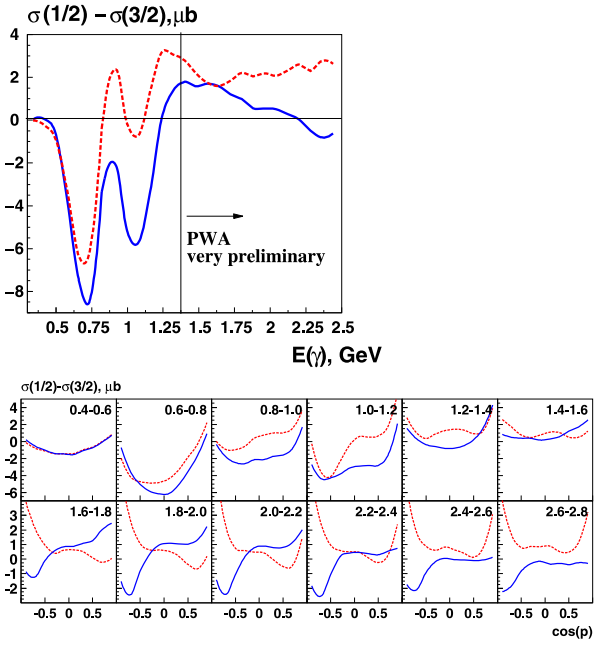

Fig. 12. Predictions for the helicity differences $\sigma_{1/2} - \sigma_{3/2}$ from the BnGa-PWA for the two ambiguous solutions where the $D_{33}(1700)$ might either decay dominantly via ℓ=0 (dashed, red) or ℓ=2 (solid, blue) into $\Delta\pi$.

2.3.3 Preliminary results

With the Crystal-Barrel/TAPS Experiment at ELSA data with a longitudinally polarised target and circularly or linearly polarised photons have been taken. The according cross section for the reactions $\vec{\gamma}\,\tilde{p} \rightarrow p\pi^0\pi^0$ and $\vec{\gamma}\,\tilde{p} \rightarrow p\pi^0\eta$ can be written as follows[18] (the polarisation of the recoiling nucleon is not measured):

$$\frac{d\sigma}{dx_i} = \sigma_0\{(1-\Lambda_z\cdot P_z)+\delta_\odot(I^\odot-\Lambda_z\cdot E)- \delta_l[\sin2\varphi(I^s-\Lambda_z\cdot G)+ \cos2\varphi(\Sigma-\Lambda_z\cdot P_z{}^c)]\},$$

where Λ_z denotes the longitudinal polarisation of the initial nucleon. $\delta_\odot$ is the degree of circular polarisation of the photon beam, while δ_l is the degree of linear polarisation, with the direction of polarisation being at an angle φ. Therefore the presently performed measurements give access to the following 7 polarisation observables: P_z, $I^\odot$, E, I^s, G, Σ, $P_z{}^c$. In the $\gamma p \rightarrow p\pi^0\pi^0$-channel for four of these polarisation observables no data exist, for most of the others the existing data is very scarce, resticted in energy, and mostly also limited significantly in the covered phase space. For $\gamma p \rightarrow p\pi^0\eta$ the only polarisation observable out of the seven, for which data exists is the beam polarisation Σ, which has been discussed in section 10.

The data taken recently at ELSA cover almost the complete solid angle and provide for the measurements with circularly polarised photons data up to $E_\gamma = 2.3$ GeV, and for the measurements with linearly polarised photons it covers the energy range from $E_\gamma = 0.5-1.35$ GeV. One example of part of the data taken with circularly polarised photons is shown in Fig. 13. Here the count rate difference between events with helicity 1/2 and helicity 3/2 is shown.

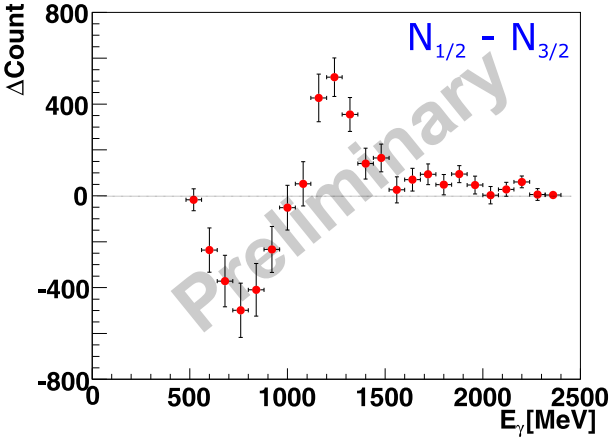

Fig. 13. Count rate difference between events with helicity 1/2 ($N_{1/2}$) and helicity 3/2 ($N_{3/2}$). The data are not corrected for acceptance, nor has the polarisation or the flux been taken into account, pure raw count rate differences are shown (very preliminary).

Non-zero count rate differences are observed. The data shown in Fig. 13 are not corrected for acceptance, nor has the polarisation or the flux been taken into account, pure raw count rate differences are shown (very preliminary). These count rate differences show structures; $N_{3/2}$ is larger than $N_{1/2}$ at lower energies, while at energies around 1250 MeV the data indicate that $N_{1/2}$ is larger than $N_{3/2}$.

This measurement, the data obtained on the double polarisation observable G and the new single polarisation observables will clearly provide new and important information for the partial wave analyses. They will resolve ambiguities in the present solutions as the one shown in Fig. 12. Given the importance of the p2π channel as inelastic channel for any coupled

channel partial wave analysis this data will provide especially valuable information. In addition, the $\gamma p \to p\pi^0\pi^0$ and the $\gamma p \to p\pi^0\eta$ final states allow the investigation of new decay modes e.g. via higher mass resonances and may therefore give access to new states or allow the determination of so far unknown properties of already known baryon resonances.

We acknowledge financial support from the Deutsche Forschungsgemeinschaft (DFG) within SFB/TR16.

References

1 Capstick S, Isgur N. Phys. Rev. D, 1986, **34**: 2809
2 Glozman L Y et al. Phys. Rev. D, 1998, **58**: 094030
3 Löring U et al. Eur. Phys. J. A, 2001, **10**: 395–447
4 Capstick S, Roberts W. Prog. Part. Nucl. Phys., 2000, **45**: S241
5 Oset E et al. Int. J. Mod. Phys. A, 2005, **20**: 1619
6 Döring M, Oset E, Strottman D. Phys. Rev. C, 2006, **73**: 045209
7 Lutz M F M, Kolomeitsev E E. Nucl. Phys. A, 2005, **755**: 29
8 Thoma U et al. Phys. Lett. B, 2008, **659**: 87
9 This conference, contribution of Sarantsev A
10 Sarantsev A V et al. Phys. Lett. B, 2008, **659**: 94
11 Prakhov S et al. Phys. Rev. C, 2004, **69**: 045202
12 Amsler C et al (Particle Data Group). Phys. Lett. B, 2008, **667**: 1
13 Horn I et al. Eur. Phys. J. A, 2008, **38**: 173
14 Horn I et al. Phys. Rev. Lett., 2008, **101**: 202002
15 Chiang W T, Tabakin F. Phys. Rev. C, 1997, **55**: 2054
16 This conference, contribution of Beck R
17 This conference, contribution of Schmieden H
18 Roberts W, Oed T. Phys. Rev. C, 2005, **71**: 055201
19 Strauch S et al. Phys. Rev. Lett., 2005, **95**: 162003
20 Hillert W. Eur. Phys. J. A, 2006, **28S1**: 139
21 Elsner D et al. Eur. Phys. J. A, 2009, **39**: 373
22 Sokhoyan V. PhD thesis, Universität Bonn (in preparation)
23 Assafiri Y et al. Phys. Rev. Lett., 2003, **90**: 222001
24 Gutz E, Sokhoyan V, van Pee H et al. Eur. Phys. J. A, 2008, **35**: 291
25 Gutz E. PhD thesis, Universität Bonn (in preparation)
26 Ajaka J et al. Phys. Rev. Lett., 2008, **100**: 052003
27 Anisovich A V et al. Eur. Phys. J. A, 2005, **24**: 111
28 Anisovich A V et al. Eur. Phys. J. A, 2007, **34**: 243
29 Bradtke et al. NIM A, 1999, **436**: 430
30 Aker E et al. Nucl. Instrum. Meth. A, 1992, **321**: 69